

Citation for published version: Cheng, S, Gu, C, Yang, X, Li, S, Fang, L & Li, F 2022, 'Network Pricing for Multi-Energy Systems under Longterm Load Growth Uncertainty', *IEEE Transactions on Smart Grid*, vol. 13, no. 4, 9734759, pp. 2715 - 2729. https://doi.org/10.1109/TSG.2022.3159647

DOI:

10.1109/TSG.2022.3159647

Publication date: 2022

Document Version Peer reviewed version

Link to publication

© 2022 IEEE. Personal use of this material is permitted. Permission from IEEE must be obtained for all other users, including reprinting/ republishing this material for advertising or promotional purposes, creating new collective works for resale or redistribution to servers or lists, or reuse of any copyrighted components of this work in other works.

University of Bath

Alternative formats

If you require this document in an alternative format, please contact: openaccess@bath.ac.uk

Copyright and moral rights for the publications made accessible in the public portal are retained by the authors and/or other copyright owners and it is a condition of accessing publications that users recognise and abide by the legal requirements associated with these rights.

Take down policyIf you believe that this document breaches copyright please contact us providing details, and we will remove access to the work immediately and investigate your claim.

Download date: 07 Mar 2023

Network Pricing for Multi-Energy Systems under Long-term Load Growth Uncertainty

Shuang Cheng, Student Member, IEEE, Chenghong Gu, Member, IEEE, Xinhe Yang, Shuangqi Li, Lurui Fang, Member, IEEE, Furong Li, Senior Member, IEEE

Abstract—The long-term uncertainty of multi-energy demand poses significant challenges to the coordinated pricing of multiple energy systems (MES). This paper proposes an integrated network pricing methodology for MES based on the long-run-incremental cost (LRIC) to recover network investment costs, affecting the siting and sizing of future distributed energy resources (DERs) and incentivizing the efficient utilization of MES. The stochasticity of multi-energy demand growth is captured by the Geometric Brownian Motion (GBM)-based model. Then, it is integrated with a system operation model to minimize operation costs, considering low-carbon targets and flexible demand. Thereafter, the kernel density estimation (KDE) method is used to perform the probabilistic optimal energy flow (POEF) to obtain energy flows under uncertain load conditions. Based on the probability density functions (PDFs) of energy flows, an LRIC-based network pricing model is designed, where Tail Value at Risk (TVaR) is used to model the risks of loading levels of branches and pipelines. The performance of the proposed methodology is validated on a typical MES. The proposed pricing method can stimulate cost-effective planning and utilization of MES infrastructures under long-term uncertainty, thus helping reduce low-carbon transition costs.

Index Terms— Flexible demand, long-run-incremental cost pricing, multi-energy system, network pricing, uncertainty.

Nomenclature

Abbreviations	A
AMISE	Approximate Mean Integrated Squared error
AQ	Annual Consumption
CDF	Cumulative Distribution Functions
CHP	Combined Heat and Power
DER	Distributed Energy Resource
D-LRIC	Deterministic Long-Run-Incremental Cost
EB	Electric Boiler
GBM	Geometric Brownian Motion
LDZ	Local Distribution Zone
LRIC	Long-Run-Incremental Cost
KDE	Kernel Density Estimation
MCS	Monte Carlo Simulation
MES	Multiple Energy Systems
MIP	Mixed-Integer Programming
PDF	Probability Density Function
POEF	Probabilistic Optimal Energy Flow
PV	Photovoltaic

Manuscript received June 27, 2021; revised October 22, 2021 and January 25, 2022; received March 07, 2022. Paper no. TSG-01017-2021 (Corresponding author: Chenghong Gu)

S. Cheng, C. Gu, X. Yang, S. Li, L. Fang, and F. Li are with the department of Electrical and Electronic Engineering, University of Bath, Bath BA2 7AY, (e-mail: sc2791@bath.ac.uk; c.gu@bath.ac.uk: yangxinhe333@gmail.com; sqli9966@gmail.com; Lurui.Fang@xjtlu.edu.cn; f.li@bath.ac.uk).

TVaR Tail Value at Risk

Indices and Sea	ts
i	Index of electricity generation units

Index of time periods during the investment horizon t b, Ω^B Index and set of electrical buses c, Ω^c Index of network component h, Ω^{DT} Index and set of time periods in a day j, Ω^{CHP} Index and set of CHP l, Ω^{line} Index and set of electrical branches o, Ω^G Index and set of gas nodes p, Ω^P Index and set of gas pipelines q, Ω^{EB} Index and set of EB s, Ω^{GS} Index and set of gas wells Ω^{Flex} Set of flexible load nodes

 Ω^{TU} , Ω^{GU} Sets of non-gas-fired and gas-fired generating units

Λ Set of compressors

Parameters

d	Discount rate
\dot{m}^c	Mass flow rate of pipelines connected from load
	node c to the source node.
r	Annuity factor
12	Gas price

Solar panel efficiency

Gas price The drift in GBM μ The volatility in GBM σ Compressor factor ω

Efficiency of the energy device η

Energy flow

Simulation parameters of PV production φ_G, σ_G Air density and area swept by WT blades ρ_b, A_b

Carbon emission coefficients of thermal units, gas $\varepsilon_T, \varepsilon_g, \varepsilon_C$

Coefficients of power and heat generation of CHP γ_H, γ_P

Price of scheduling flexible demand Ramp rate limit of the generating unit Gas flow constant of the gas pipeline

 η^{ge} , η^{gh} Efficiency of CHP from gas to electricity and from

gas to heat.

Voltage angle

Array surface area in square meters

Bus-branch and bus-generator incidence matrix B.M.NCHP-bus, CHP-gas node and CHP-heating source

incidence matrix

CaCapacity of the network component

C_{P}	Power coefficient of WT
C,I	Node-gas source and node-gas pipeline incidence
=	matrix
\overline{F}	Maximum supply of gas well
H,K	EB-bus and EB-heating source incidence matrix
G_0,G_g	Extra-terrestrial and global horizontal radiation
P_{max}^G, P_{unit}^G	Maximum and minimum power output of generating
Trease acres	units
R	Gas-fired unit-gas node incidence matrix
$T_{min}^{on}, T_{min}^{off}$	Minimum start-up and shutdown time of generating
men. min	units
V_{wt}	Wind speed
$\frac{V_{wt}}{V_{CHP}}, \overline{V_{EB}}$	Maximum gas input of CHP and electricity input of
CHP, EB	EB
Z_l	Impedance of electricity line
•	
Variables	
E^{Ele} , E^{Gas}	Electricity input of EB and gas input of CHP
	Electricity input of EB and gas input of CHP Gas supply of gas source
E^{Ele} , E^{Gas}	
E ^{Ele} ,E ^{Gas} F ^{GS} F	Gas supply of gas source
E^{Ele} , E^{Gas} F^{GS} f^{line} , f^{gas}	Gas supply of gas source Energy flow
E ^{Ele} ,E ^{Gas} F ^{GS} F	Gas supply of gas source Energy flow Power flow and gas flow
E^{Ele} , E^{Gas} F^{GS} F f f^{line} , f^{gas} g H^{CHP}	Gas supply of gas source Energy flow Power flow and gas flow Gas production from the gas well
E^{Ele} , E^{Gas} F^{GS} f^{line} , f^{gas}	Gas supply of gas source Energy flow Power flow and gas flow Gas production from the gas well Heat power generated by CHP
E^{Ele} , E^{Gas} F^{GS} F f f^{line} , f^{gas} g H^{CHP} h_s K	Gas supply of gas source Energy flow Power flow and gas flow Gas production from the gas well Heat power generated by CHP Bandwidth of the kernel estimator Kernel function
E^{Ele} , E^{Gas} F^{GS} F f f^{line} , f^{gas} g H^{CHP} h_s	Gas supply of gas source Energy flow Power flow and gas flow Gas production from the gas well Heat power generated by CHP Bandwidth of the kernel estimator Kernel function
E^{Ele} , E^{Gas} F^{GS} F f f^{line} , f^{gas} g H^{CHP} h_s K L^{ED} , L^{GD} , L^{HD}	Gas supply of gas source Energy flow Power flow and gas flow Gas production from the gas well Heat power generated by CHP Bandwidth of the kernel estimator Kernel function Electricity, gas and heat demand
E^{Ele} , E^{Gas} F^{GS} F f^{line} , f^{gas} g H^{CHP} h_s K L^{ED} , L^{GD} , L^{HD} L^{Ele}	Gas supply of gas source Energy flow Power flow and gas flow Gas production from the gas well Heat power generated by CHP Bandwidth of the kernel estimator Kernel function Electricity, gas and heat demand Electricity production of CHP Sample capacity of the kernel estimator
E^{Ele} , E^{Gas} F^{GS} F f^{line} , f^{gas} g H^{CHP} h_s K L^{ED} , L^{GD} , L^{HD} L^{Ele} n	Gas supply of gas source Energy flow Power flow and gas flow Gas production from the gas well Heat power generated by CHP Bandwidth of the kernel estimator Kernel function Electricity, gas and heat demand Electricity production of CHP

I. INTRODUCTION

Peak demand growth rate at time t

Lower and upper limits of the nodal gas pressure

AKDE independent variable

Nodal gas pressure

x

x(t)

 π_p , $\overline{\pi_p}$

MULTI-energy systems have been recognized as a costeffective way to create a sustainable and low-carbon future. Although significant research has been conducted to unlock the potential of MES, the uncertainty of the siting and sizing of future energy demand and DERs makes it difficult to plan MES [1]. The uncertainty can also lead to a high likelihood of overinvestment and inefficient utilization of infrastructure [2]. For example, as reported by National Grid UK [3], peak electricity demand could rise by between 5 and 8.1 GWs by 2030 to meet its 2050 carbon reduction target.

Many factors can cause long-term uncertainty in MES planning, e.g., load growth, generation expansion, market rules, etc. Load growth uncertainty has been regarded as one of the most crucial determinants [4], which can cause great risks for MES planners and investors. It is extensively investigated in this paper. Some references have investigated MES load uncertainty modelling approaches. Reference [5] simulates the dynamics of uncertain customers through a Markov decision process (MDP) method. The proposed method enables system operators to parameterize and model multi-energy dynamics in MES dispatching. However, this paper is focused on short-term uncertainty rather than long-term demand growth. Reference [6] models the uncertainties of energy carrier demand response and various load types in MES by a 2m+1 point estimate

strategy. It simulates the random behaviors of multi-energy demand but also ignores long-term load growth uncertainty. Paper [7] resolves the uncertainties of electricity and thermal load through a scenario-based multistage adaptive stochastic optimization approach. It can enable networks to accommodate more uncertain load in the short term. Most papers focus on the uncertainty of load shifting between multiple energy carriers, but to the best of the authors' knowledge, the multi-energy load growth uncertainty has not been well investigated in MES planning and pricing.

Some papers incorporate uncertainties in optimal MES planning. Reference [8] proposes an expansion planning model to minimize the total costs of investment, operation, potential risks under uncertainty and unserved energy. Nevertheless, only the uncertainty of wind power generation is modelled. Paper [9] addresses MES optimal planning by considering the uncertainty of net load demand. Reference [10] proposes a unified operation and planning method to quantify the flexibility value under long-term price uncertainties. However, these papers passively design the planning methodology with stochastic models instead of proactively guiding the system development and increasing the utilization of network infrastructures.

To efficiently utilize MES, economic incentives [11] can be used to guide the sizing and siting of future demand and DERs. Reference [12] formulates a forward-looking clearing and pricing framework for day-ahead markets to integrate gas and electricity systems. Reference [13] investigates dynamic pricing by developing a two-leader multi-follower bi-level model. However, these models aim to allocate resources and ensure energy balance efficiently in the wholesale market. Infrastructure investment is not considered in the short-term pricing mechanisms. In terms of long-term pricing approaches in the gas system, Local Distribution Zone (LDZ) customer charges [14] are adopted in natural gas systems through a consumption-relevant three-tier pricing method. The method can be divided into three categories based on the capacity charge for supply points and the fixed charge depending on the meter reading. However, the charging method is simplified by ignoring the impact of nodal incremental demand on the utilization of the gas network since it assumes that the system is fully utilized. Regarding heating networks, there is no nationally regulated heating pricing method [15]. In most cases, a dual tariff scheme is applied to district heating based on fixed investment costs and variable fees (e.g., fuel purchase).

Use-of-system (UoS) charge is one such economic signal to recover network investment costs and affect network use by customers [16]. Forward cost pricing (FCP) [17] calculates the zonal network prices by dividing the distribution network into isolated groups, using zonal charges to recover the expected costs of network reinforcement. The LRIC method is a forward-looking system charging method for electricity systems to quantify the discounted future reinforcement cost due to incremental nodal energy demand and allocate investment costs [18]. It reflects both the capacity-related cost and the degree to which the network is utilized. However, its accuracy and efficacy are challenged with more volatile load growth. To accommodate uncertain load growth, reference [19] develops a

novel network pricing method based on the fuzzy model. Paper [20] proposes a probabilistic model to quantify the demand-side uncertainty and incorporate it into the network pricing model to incentivize uncertainty reduction. Adopting LRIC in MES pricing can provide coordinative forward-looking price signals.

It is challenging to represent the effects of uncertainty [21] in LRIC. Traditional LRIC ignores uncertainties and regards electricity demand as deterministic, which misleads MES planning due to inaccurate cost-reflective signals. Therefore, the unbalanced distribution of DERs and demand [22] not only encourages excessive investment but also impedes decarbonization.

Considering power flows with and without nodal energy increments are key factors in the traditional LRIC method, stochastic energy flows are required to address MES network pricing under long-term uncertainty. Probabilistic energy flow is one of the most powerful tools to analyze MES with volatile generation and demand. Generally, there are three methods to solve probabilistic energy flow problems [23]: Monte Carlo simulation (MCS), analytical methods, and estimation methods [24]. Based on numerous iterations, MCS has high computational costs. In terms of analytical methods, the strict assumptions that the system states and output variables have normal density functions inhibit their applications to complicated energy systems [25]. Even though point estimation methods solve the computational problem, they cannot provide PDFs of the estimated random variables [26]. In comparison, the KDE method can generate nonparametric PDFs for complex systems in an easy manner. However, the fixed KDE has [27] low accuracy to capture long-tailed distributions. Adaptive KDE methods with variable bandwidth are more efficient to capture the long-tails and thus provide a satisfactory estimation.

In summary, the drawbacks of existing literature are: 1) Most literature emphasizes the uncertainty of multi-energy load shifting and short-term demand uncertainty in MES. The uncertainty of long-term load growth has not been investigated in MES planning and pricing. 2) In terms of probabilistic energy flow modelling, the computation burden of MCS, strict assumptions of analytical methods and long-tailed distribution problems of fixed KDE methods cannot provide satisfactory results. 3) Most research focuses on MES optimal planning under uncertainty, which passively react to future generation/demand. There are no long-term MES pricing models to proactively plan networks through economic signals.

To fill the gap in network pricing and probabilistic energy flow calculation for MES, this paper develops an LRIC oriented pricing method for MES. The proposed methodology aims at filling these gaps by modelling GBM-based demand uncertainty in long run, estimating probabilistic optimal energy flows through adaptive KDE, and integrating LRIC in MES network planning. Firstly, a stochastic model based on GBM [28] is designed to model uncertainties of energy demand growth. The GBM approximation can capture the load growth uncertainty, considering the time value of deferring investment. The GBM simulation presents that the demand uncertainty would increase as time elapses, which is aligned with the current situation that, due to the emergence of new

technologies, the accuracy of load forecast reduces over time. The variables are parameterized to incorporate the impacts of the paradigm shift in energy system load based on the Future Energy Scenarios in [3].

This paper develops a POEF model, based on the PDF of load growth. PDFs of energy load growth are input to the system operation model to minimize the total costs of energy supply, scheduling flexible demand and carbon emissions. The POEF model adopts a non-parametric method, i.e., adaptive KDE [29], to capture probabilistic energy flows. It can not only reduce the computational time but also obtain complete PDFs of energy flows. Compared to other models, the adaptive KDE-based model has the following advantages: 1) It has a better fitting effect for datasets with long-tailed distributions; 2) It is more effective to provide the PDFs of datasets with non-normal distributions; 3) It does not require strict assumptions and thus is easy to implement in a complex energy system.

With probabilistic energy flows, TVaR [30] [31] is adopted to derive the expected overloading levels of network components under long-term uncertainty. Thereafter, an LRIC-based network pricing method is designed, derived from the present value differences with and without nodal energy withdrawal and injection. Different from short-term pricing models (e.g., locational marginal pricing) [32] [33], the proposed pricing method can produce forward-looking nodal UoS charges that not only reflect the utilization of MES but affect the sizing and siting of customers. Therefore, it can stimulate efficient utilization of MES, thus enabling network planners to de-risk investment by strategically managing the system capacity. The main contributions of this paper are:

- It for the first time proposes a new GBM-based stochastic model for uncertain multi-energy load growth in the long term, considering the changing variances over time. Existing uncertainty modelling methods [5] [6] [7] [20] only accommodate uncertain load dynamics in the short term. The proposed method emphasizes the demand growth uncertainty, which has been regarded as one of the most crucial determinants in MES planning. Such a model has a lognormal probability density function to better capture the skewness of load growth uncertainty. Unlike fixed variance models [10], the proposed method adopts variable variances to reflect the fact that from the point of prediction, as time elapses, the accuracy of load forecast would decrease. The results demonstrate that the simulated demand growth trajectories can better align with and sufficiently disperse around their averages to incorporate future scenarios. Thus, it can better capture the long-term stochasticity of the multienergy demand growth.
- It designs a novel POEF model by the non-parametric estimation method, i.e., adaptive KDE. It can obtain PDFs of MES flow variables easily. The high computational costs of MCS [34] and strict assumptions of analytical methods [25] interfere with their applications in complex MES. Although the fixed KDE estimation approach [27] has reasonable accuracy and needs low computation, it cannot effectively estimate the long-tails of density functions. In comparison, the proposed adaptive KDE model uses variable bandwidth to achieve a better fitting effect for

datasets with long-tailed distributions. Moreover, it is more effective to provide PDFs of datasets with a much lower deviation for non-normal distributions.

• It for the first time proposes a coordinative long-term forward-looking pricing model in MES, where TVaR is adopted to quantify the average value of expected energy flows at risk. It distinguishes price signals based on load growth uncertainty and network utilization levels. Different from short-term price signals [32] [33] to satisfy allocative operational efficiency, the proposed pricing model enables rational utilization of existing systems and efficient MES planning. Unlike other long-term pricing methods, e.g., the zonal pricing method FCP [17], and the three-tier consumption-relevant pricing method [14], the LRIC approach can reasonably reflect the effect of nodal incremental multi-energy demand on the predicted investment horizons of branches and pipelines. Thus, it is more cost-reflective to incentivize effective sitting and sizing of future demand. Compared with the deterministic LRIC method, it shows a better performance to address demand growth uncertainty.

The remainder of this paper is organized as follows. Section II presents the detailed formulation of MES. Section III formulates the LRIC-based pricing model. Section IV demonstrates the implementation of the proposed method. Section V validates the efficacy of the proposed method. The conclusions are drawn in Section VI.

II. MODELLING OF MES

This section demonstrates the detailed formulation of MES, including the stochastic model and the system operation model.

A. Stochastic Modeling of load growth and DERs

1) Stochastic modelling of load growth

Considering the risk of future load fluctuations, the GBM model [35] is used to capture the long-term stochastic behaviour of load growth rates, as shown in (1).

$$dx(t) = x(t)[\mu dt + \sigma dB(t)], x_0 = x(0)$$
 (1)

where the drift μ denotes the instantaneous conditional expected percentage change in x per unit time; σ is the instantaneous conditional standard deviation per unit time; dB(t) represents a standard Brownian motion (i.e., Wiener process). The energy systems with higher levels of μ have a bigger load growth, while those with higher levels of σ are characterized by greater uncertainty over the whole investment horizon. Therefore, by solving the Fokker-Planck equation of (1), the PDF of load growth rates can be derived, as shown in (2). The corresponding expected value and variance are given by (3) and (4). The variable growth rates x(t) has a lognormal distribution with parameters $\ln x_0 + \bar{\mu}t$ and $\sigma\sqrt{t}$.

$$f(x,t) = \frac{1}{x\sigma\sqrt{2\pi t}}e^{-(\frac{(\ln x - \ln x_0 - \overline{\mu}t)^2}{2\sigma^2 t})}, \overline{\mu} = \mu - \frac{\sigma^2}{2}$$
 (2)

$$E(x(t)) = x_0 e^{\mu t + \frac{\sigma^2 t}{2}}$$
 (3)

$$Var(x(t)) = x_0^2 e^{2\mu t + \sigma^2 t} (e^{\sigma^2 t} - 1)$$
 (4)

2) DER modelling

In this paper, photovoltaics (PV) and wind turbines (WTs) are considered as DERs. The output power of PV and extracted wind power are shown as (5) and (6):

$$PV = \alpha \times A_s \times G_0 \times \int_0^1 f(G_g/G_0; \varphi_G; \sigma_G)$$
 (5)

$$WT = \frac{1}{2} C_P \rho_b A_b V_{wt}^3 \tag{6}$$

where the global horizon radiation G_g is scaled into [0,1]. Parameters φ_G and σ_G are estimated through fitting Beta distribution into the historical solar irradiance. The variable of the integral part is $\frac{G_g}{G_0}$, whose probability function is estimated from the pre-determined parameters φ_G and σ_G . Since short-term DER uncertainty is not the main driver of MES network reinforcement [36], the parameters of equations (5) and (6) remain the same for the time horizon to provide a typical hourly renewable output curve.

B. System Operation Model

To investigate the optimal energy flow, this part formulates the economic and low-carbon operation model of MES to minimize the electricity generation costs, natural gas purchase costs and carbon emission costs, as follows:

$$min \sum_{h \in \Omega^{DT}} C^g + C^{gas} + C^{flex} + C^c$$
 (7)

$$C^{g} = \sum_{i \in \Omega^{TU}} \left(a_{i} + b_{i} P_{i,h}^{G} + c_{i} P_{i,h}^{G^{2}} \right)$$
 (8)

$$C^{gas} = \sum_{s \in \Omega} Gs(v_s g_{s,h}) \tag{9}$$

$$C^{flex} = \sum_{b \in O^{Flex}} (\delta_b | P_{b,h}^{Flex} |)$$
 (10)

$$C^{c} = k \left[\sum_{i \in \Omega^{TU}} (\varepsilon_{T} P_{i,h}^{G}) + \sum_{i \in \Omega^{GU}} (\varepsilon_{g} P_{i,h}^{G}) + \sum_{i \in \Omega^{CHP}} \varepsilon_{C} (\gamma_{P} P_{i,h}^{G} + \gamma_{H} H_{i,h}^{CHP}) \right].$$
(11)

Equation (7) aims to minimize the total operating costs. The first term (8) is the operation cost of non-gas-fired thermal generators, which is a quadratic function. The second term (9) is gas production costs from gas wells. The third item (10) denotes the total scheduling costs of flexile demand, which is the product of scheduling price and scheduled power. The fourth term (11) is the total carbon emission costs of non-gas-fired thermal generators, gas-fired generators and CHP units. γ_P and γ_H are the coefficients that describe the relationships between fuel consumption and power and heat productions of CHP, respectively.

The objective function is subject to the following constraints.

1) Power system constraints

$$P_{min,i}^G \leq P_{i,h}^G \leq P_{max,i}^G, h \in \Omega^{DT}, \forall i \in \Omega^{TU} \cup \Omega^{GU}$$
 (12)

$$\left| P_{i,h}^G - P_{i,h-1}^G \right| \le r_{gi} \tag{13}$$

$$T_{i,h}^{on} \ge T_{min}^{on}, T_{i,h}^{off} \ge T_{min}^{off}, \forall h \in \Omega^{DT}, \forall i$$

$$\in \Omega^{TU} \cup \Omega^{GU}$$
(14)

$$\sum_{i \in \Omega_{b}^{TU} \cup \Omega_{b}^{GU}} G_{b,i} P_{i,h}^{G} + \sum_{j \in \Omega_{b}^{CHP}} B_{j,b} L_{j,h}^{Ele} +$$

$$\sum_{l \in \Omega^{line}} A_{b,l} f_{l,h}^{line} = L_{b,h}^{ED} - P_{b,h}^{Flex} +$$

$$\sum_{q \in \Omega_{b}^{EB}} H_{q,b} E_{q,h}^{Ele}, \forall b \in \Omega^{B}, \forall h \in \Omega^{DT}$$

$$(15)$$

$$f_{lh}^{line} = (\theta_{mh} - \theta_{nh})/Z_l \tag{16}$$

where Ω_b^{TU} Ω_b^{GU} , Ω_b^{EB} and Ω_b^{CHP} are the set of non-gas-fired thermal units, gas-fired thermal units, EB units and CHP units at bus b, respectively.

Constraint (12) enforces the capacity constraints of electricity generation units. Constraints (13) and (14) denote the ramp up and ramp down constraints and the minimum start-up and shutdown constraints for generating units, respectively. Constraint (15) ensure the nodal electricity load balance. The direct-current (DC) power flow is used, as shown in (16). It defines the power flow through electricity line $l. f_{l,h}^{line}$ is the power flow in line l at time h. $\theta_{m,h}$ and $\theta_{n,h}$ are the voltage angles of the two end nodes of line l at time h, respectively. Z_l is the impedance in line l. The line power flow constraints are ignored in the operation model but considered in the pricing model. To calculate the cost of advancing or deferring future investment with nodal demand injection, the expected reinforcement year should be derived when the line power flows exceed a threshold. This process inherently enforces line capacity constraints to the proposed pricing approach and is demonstrated in Part B of Section III.

2) Gas system constraints

$$\begin{split} & \sum_{p \in \Omega^P} I_{o,p} f_{p,h}^{gas} + \sum_{s \in \Omega^{GS}} C_{o,s} F_{s,h}^{GS} = L_{o,h}^{GD} + \\ & \sum_{\in \Omega^{CHP}} M_{j,o} E_{j,h}^{Gas} + \sum_{i \in \Omega^{GU}} R_{i,o} \frac{P_{i,h}^G}{\eta_i}, \forall o \in \\ & \Omega^G, \forall h \in \Omega^{DT} \end{split} \tag{17}$$

$$0 \le F_{sh}^{GS} \le \overline{F_s}, \forall s \in \Omega^{GS}, \forall h \in \Omega^{DT}$$
 (18)

$$f_{pm,h}^{gas} = \phi_{pm} sign(\pi_{p,h}, \pi_{m,h}) \sqrt{(\pi_{p,h})^2 - \pi_{m,h}^2}$$

$$\forall (p,m) \in \Omega^P, \forall h \in \Omega^{DT}$$
(19)

$$\underline{\pi_o} \leq \pi_{o,h} \leq \overline{\pi_o}, \forall h \in \Omega^{DT}, \forall o \in \Omega^G$$
 (20)

$$\pi_{m,h} \le \omega \pi_{n,h}, \forall h \in \Omega^{DT}, \forall (p,m) \in \Lambda$$
 (21)

Constraint (17) is the nodal gas load balance. Constraint (18) ensures the gas supply limits of gas wells. Constraint (19) is the Weymouth equation for pipeline gas flows. Constraint (20) is the pressure limits for gas network nodes. For a gas pipeline with a compressor, constraint (21) is the pressure relationship between inlet and outlet.

3) Energy coupling constraints

The power system and natural gas system are coupled through gas-fired units and CHP, the relationship of which has been formulated in the nodal gas load balance constraint (17). In addition, (22) ensures that the electricity production of CHP is strictly fulfilled. The heating demand is coupled through CHP and EB with the electricity system and gas system, as shown in (23)-(25). Constraint (23) represents the coupling relationship of heat demand, CHP and EB, i.e., the heating production of CHP and EB is equal to the heating demand. Constraints (24) and (25) enforce the capacity constraints of CHP and EB, respectively.

$$L_{j,h}^{Ele} = \eta_{j}^{ge} E_{j,h}^{Gas}, \forall j \in \Omega^{CHP}, \forall h \in \Omega^{DT}$$
 (22)

$$F_{e,h}^{HS} = \sum_{q \in \Omega^{EB}} \eta_q E_{q,h}^{Ele} + \sum_{j \in \Omega^{CHP}} \eta_j^{gh} E_{q,h}^{Gas}, \forall e \in$$

$$\frac{\Omega^E, \forall h \in \Omega^{DT}}{0 \le E_{j,h}^{Gas} \le \overline{V_{CHP}}, \forall j \in \Omega^{CHP}, \forall h \in \Omega^{DT}}$$

$$(23)$$

$$0 \le E_{j,h}^{Gas} \le \overline{V_{CHP}}, \forall j \in \Omega^{CHP}, \forall h \in \Omega^{DT}$$
 (24)

$$0 \le E_{q,h}^{Ele} \le \overline{V_{EB}}, q \in \Omega^{EB}, \forall h \in \Omega^{DT}$$
 (25)

III. PRICING MODEL FORMULATION

This section presents the proposed probabilistic optimal energy flow model and the LRIC-based system pricing model.

Probabilistic Energy Flow Model

Given that the traditional deterministic MES operation model cannot incorporate energy system uncertainties, a POEF is required to determine the energy flows under specified loading conditions. In this section, the adaptive KDE [24] is developed to solve the POEF problem.

With the PDF of the load growth rates modelled in (2), samples are produced from historical data. Thereafter, the system operation model solves the optimal energy flows for each sample path and thus obtain the output variables, i.e., the daily optimal energy flows. Given that the maximum power flows are the driving factor for network infrastructure investment rather than the overall consumption, the maximum values are selected from the 24-hour output data to perform the KDE-based POEF model. It is assumed that $F_1, F_2, ... F_n$ is a set of maximum energy flows for components 1,2,...n with unknown PDFs. Thus, the KDE-based PDF model can be expressed as (26).

$$\hat{f}_{h_s}(x, F_c) = \frac{1}{n} \sum_{i=1}^{n} K_{h_s}(x - F_c) = \frac{1}{nh_s} \sum_{i=1}^{n} K\left(\frac{x - F_c}{h_s}\right)$$
(26)

where the bandwidth h_s is the smoothing parameter or bandwidth, i.e., a given scale parameter. It presents a strong influence on the resulting estimate. The choice of bandwidth h_s is discussed in detail below. x is the non-parametric KDE independent variable. The Kernel function $K(\cdot)$ determines the shape of bumps which are summed up to the kernel estimator, while the bandwidth h_s determines their width [24]. Selecting the Gaussian function as $K(\cdot)$, it can be expressed as (27).

$$K(x, F_c) = \frac{1}{\sqrt{2\pi}} e^{\frac{-(x - F_c)^2}{2h_s^2}}$$
 (27)

Therefore, the estimated PDF of energy flows is determined by $K(\cdot)$ and the bandwidth h_s . Particularly, the results are much more sensitive to the choice of h_s [37]. To ensure the trade-off between bias and variance of the estimator, the Approximate Mean Integrated Squared Error (AMISE) method is used to select the optimal bandwidth [25], as shown in (28) and (29).

$$AMISE = \frac{h_s^4}{4} \left\{ \int u^2 K(u) du \right\}^2 \int \{f''(x)\}^2 dx + \frac{1}{nh_s} R(K)$$
 (28)

$$R(K) = \int K^2(u)du \tag{29}$$

where f''(x) is the estimated PDF through KDE, $u = \frac{x - F_i}{h_s}$. AMISE is used to quantify the difference between true realization and estimated density function. By minimizing AMISE, the optimal bandwidth can be obtained. The Likelihood Cross-Validation method is used to find the optimal

 h_s index for each output random variable and minimize *AMISE*.

B. LRIC-based System Pricing Model

The difference in the present value of future investment with and without the nodal connection determines network charges. Based on this principle, the proposed LRIC charging model is demonstrated as follows.

1) Deriving contingent overloading

The risk measure, TVaR is used to derive the expected overloading levels of a network component c, i.e., the pipeline in the gas system and the branch in the electricity system during the whole time horizon. The time horizon T represents the time range when the system operator expects to recover the investment costs from the network users. It is necessary to select a sufficient planning horizon (7-10 years) to enable the MES operator to earn a reasonable rate of return on the capital invested. In this paper, T is selected as 10 years. Given that the PDFs of energy flows are derived above, they can be expressed as $f_{c,t_c}(\rho)$ for component c in year t. Therefore, their cumulative distribution functions (CDF) can be expressed as

$$F_{c,t_c}(\rho) = \int_{-\infty}^{\rho} f_{c,t_c}(u) du, \forall c \in \Omega^c, \forall t$$
 (30)

Therefore, the TVaR, i.e., the expected overloading level of component c in year t can be formulated as in (31).

$$TVaR_{c,t_c} = \frac{\int_{ca}^{\infty} u \cdot f_{c,t_c}(u) du}{1 - F_{c,t_c}(Ca)}, \forall c \in \Omega^c, \forall t$$
 (31)

where Ca is the capacity of c. $1 - F_{c,t_c}(Ca)$ represents the probability of overloading, i.e, when the energy flow in a network component exceeds its capacity.

2) Deriving network costs to support existing customers

As shown in Fig. 1, the shadow area is the value of $1 - F_{c,t_c}(Ca)$. With the known PDF $f_{c,t}(u)$ and the pre-set capacity Ca, the value of $\int_{Ca}^{\infty} u \cdot f_{c,t_c}(u) du$ can be calculated. Therefore, $TVaR_{c,t_c}$ can be derived from (31). With increasing power flows, $TVaR_{c,t_c}$ also increases until reaches the threshold Ca in year t_c when the reinforcement is required.

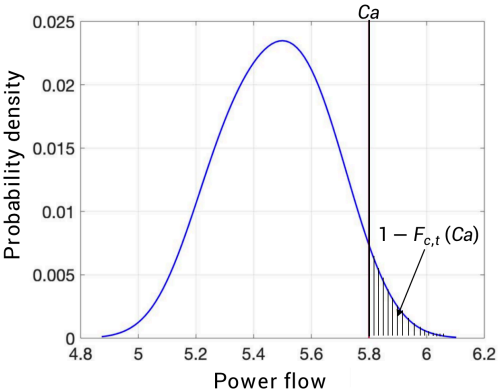


Fig. 1. Demonstration of TVaR based on known PDF.

The reinforcement of component c will be triggered when it reaches its capacity due to energy load growth. Thus, based on TVaR and the capacity Ca, the expected reinforcement time t_c can be derived by equating TVaR and the capacity of component c, as shown in (32), which can be solved through

the Newton-Raphson method.

$$TVaR_{c.t.c} = Ca (32)$$

Thereafter, the discount rate d is used to discount the future reinforcement cost $RCost_c$ to the present value as shown in (33). Notably, generation capacity investment is not considered in the proposed MES pricing model because: i) Generation investment is managed by power plants. Network distribution companies do not have the permission to invest in generation; ii) Network prices for demand are annually calculated on a rolling base, where the capacity of generation is assumed to be constant [38].

$$PV_c = \frac{RCost_c}{(1+d)^{t_c}} \tag{33}$$

3) Deriving network costs of incremental injection or withdrawal

With additional energy withdrawal ΔE at a node, the probabilistic energy flows in the system will change, as well as the TVaR. Therefore, the reinforcement time will be deferred or advanced. The TVaR along with component c due to additional energy demand or generation is

$$TVaR_{c,t_c}^{new} = \frac{\int_{Ca}^{\infty} u \cdot f_{c,t_c}^{new}(u) du}{1 - F_{c,t_c}^{new}(Ca)}, \forall c \in \Omega^c, \forall t$$
 (34)

where the PDF and CDF of energy flows are updated with incremental energy withdrawal. Therefore, the present value of the future reinforcement cost is

$$PV_c^{new} = \frac{RCost_c}{(1+d)^{t_c^{new}}}$$
 (35)

where t_c^{new} is the updated reinforcement time, which can be derived by (32) and (34).

4) Deriving LRIC charges

The change in the present value due to incremental withdrawal at node b is shown in (36), derived by (33) and (35).

$$\Delta PV_c(b) = PV_c^{new}(b) - PV_c(b)$$

$$\forall b \in \Omega^B \cup \Omega^G \cup \Omega^E$$
 (36)

Thereafter, the annuity factor r is applied to the annualized incremental costs of all components in the system, which is the LRIC charge of the node, as shown in (37).

$$LRIC(b) = \frac{\sum_{c \in \Omega^{c}} r \cdot \Delta PV_{c}(b)}{\Delta E}$$

$$, \forall b \in \Omega^{B} \cup \Omega^{G} \cup \Omega^{E}$$
(37)

where ΔE is the nodal incremental withdrawal.

IV. IMPLEMENTATION

This section illustrates the implementation of the proposed method. The stochastic model, the MES operation model, the POEF model and the LRIC-based pricing model are integrated as shown in Fig. 2. Based on the framework, Fig. 3 presents how the proposed method can be implemented. The procedures are clarified as follows:

- 1) Initialize the expected reinforcement time. The expected reinforcement time t_c for all network components is initialized as 0
- 2) Calculate probabilistic energy flows in year t_c . The PDF of uncertain load growth and system parameters are input to the

system operation model and the POEF model to calculate the PDF of the maximum energy flow in year t_c .

- 3) Calculate the expected loading level in year t_c . The expected loading level of component c, i.e., TVaR is calculated for the base case and nodal incremental case. As shown in Fig. 3, the judging criteria is the same for these two cases: If the value is smaller than the capacity and t_c is within the time horizon T, increase t_c by 1 and go back to step (2). Otherwise, go to step (4).
- 4) Calculate the incremental present value of future reinforcement cost. With the expected reinforcement time with the base case and the incremental case, their present values of future reinforcement costs are calculated. Thus, the changes in these present values, i.e., the incremental costs are obtained.
- 5) Calculate the nodal LRIC charge. The incremental costs for all network components are annualized and summed up to calculate the nodal LRIC charges.

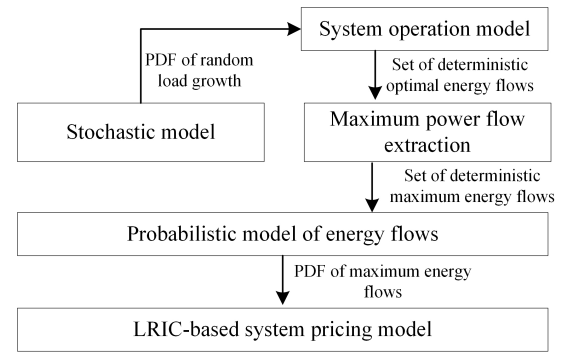


Fig. 2. Framework of the model formulation.

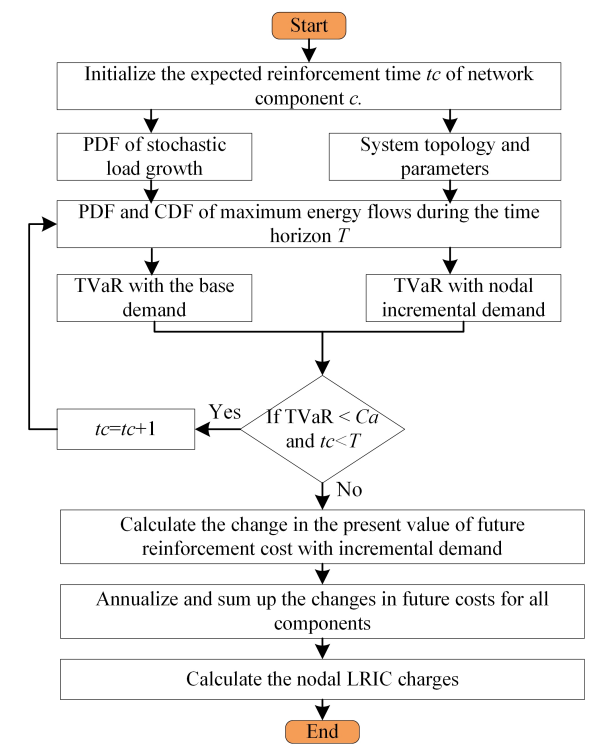


Fig. 3. Implementation of the proposed method.

V. CASE STUDY

A modified 39-bus power system and a 20-node natural gas system [39] are used to validate the effectiveness of the

proposed method. The IEEE 39-bus system is scaled down to kW to represent the district-level MES. Fig. 4. shows the topology of the system. The power system has 11 generating units, including two micro gas turbines G4 and G8 on buses 33 and 37, respectively. They are supplied by nodes N6 and N19, respectively in the gas system. Generators G4 and G8 are PV and WT, respectively. The others are diesel generating units. The cost functions of gas-fired and diesel generators are quadratic. The total generation capacity of the power system is 7367kW. Buses 3, 4, 5, 6, 7, 8, 9 have flexible demands, the capacity of which are shown in Table I. The upper limits denote the maximum volumes of load increasing, while the lower limits denote the maximum volumes of load shedding.

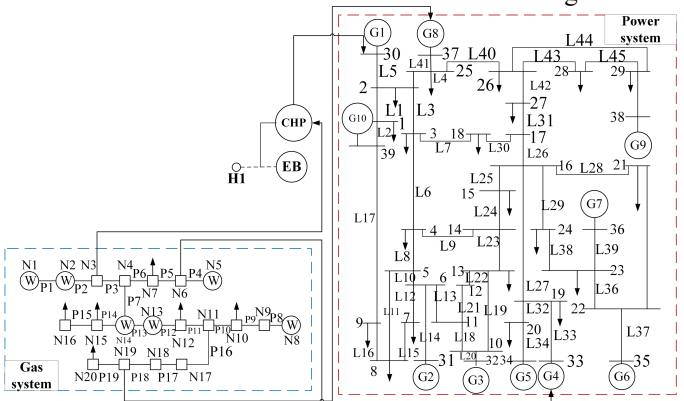


Fig. 4. Topology of the system.

TABLE I PARAMETERS OF FLEXIBLE DEMAND

	THREE PER OF TEE INDEED BEAUTY			
Bus	Upper limits of controllable	Lower limits of controllable		
	demand/kW	demands/kW		
3	150	-100		
4	150	-100		
7	150	-100		
8	100	-60		
9	350	-200		

The 20-node gas system has 6 gas wells and 18 pipelines. There are 9 gas loads, with nodes N3, N6, and N19 supplying the CHP, the gas-fired generator G4 and G8, respectively. The CHP and EB are connected with the heating load H1. The EB is connected with Bus 24 in the power system. The capacity parameters of the gas wells are shown in Table II. The parameters of the stochastic model and the network charging model are shown in Table III. Considering the MES operation model is a complicated and constrained nonlinear optimization problem, it is solved by Gurobi 9.1.0. The mixed-integer programming (MIP) optimality gap is set as 10⁻⁶. All case studies are implemented by MATLAB 2019 on a PC with Intel Core i7/2.2-GHz-based processor and 16 GB of RAM.

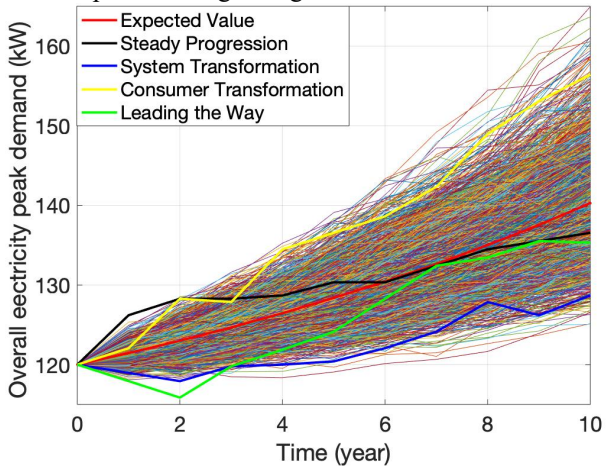
TABLE II

PARAMETERS OF GAS WELLS			
Gas well	Production	Upper limits	Lower limits
	costs	$/10^{6} Mm^{3}$	$/10^{6} Mm^{3}$
	$/\text{£}\cdot Mm^{-3}$		
W1	0.085	1.7391	0.9
W2	0.085	1.26	0
W3	0.085	0.72	0
W4	0.062	2.3018	1
W5	0.062	0.27	0
W6	0.062	1.44	0

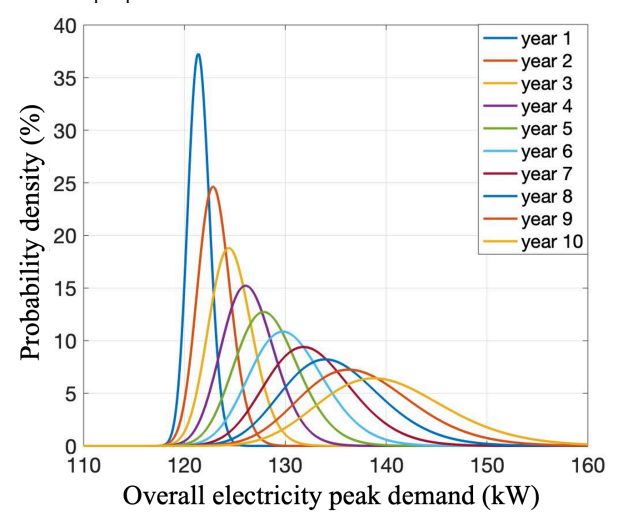
TABLE III SIMULATION PARAMETERS

Parameter	Value
Initial electricity load growth rate	0.2
The percentage drift μ for electricity load	0.07
The percentage volatility σ for electricity load	0.05
Initial gas load growth rate	0.03
The percentage drift μ for gas load	0.08
The percentage volatility σ for gas load	0.07
Investment cost of electricity branches	$70,964 \text{ £} \cdot \text{kW}^{-1}$
Investment cost of pipelines	1,750,000 £
Discount rate	6.9%

According to the predicted demand growth in National Grid's annual future energy scenarios report [3], the total electricity peak demand is simulated through the GBM model as an example. The simulated sample paths and PDFs are illustrated in Fig. 5 (a) and (b), respectively. It can be found that load uncertainty has a positive correlation with the time horizon. With the accuracy of load predicting declining over time, the variance of electricity peak demands becomes greater, illustrating the characteristics of long-term uncertainty. The gas demand growth rates are modelled using the same model but with different parameters, as shown in Table III. The values of the drift and the volatility are determined by referring to the report [3]. Remarkably, as predicted by National Grid in [3], the peak gas demand is quite likely to show a downward trend. Thus, the parameters of the gas demand growth are chosen to capture the potential negative growth scenarios.



(a) Realizations of GBM-based overall electricity peak demand in 10 years. Simulated sample paths are 2000.



(b) Probability density distribution of overall electricity peak demand

Fig. 5. Overall electricity peak demand based on the proposed stochastic model. $\mu=0.07$. $\sigma=0.05$. $x_0=0.2$. The original demand in year 0 is 100 kW.

As shown in Fig. 5 (a), the red line represents the expected load growth. The black, blue, yellow, and green lines represent the peak demand growth in four scenarios (i.e., steady progression, system transformation, consumer transformation, and leading the way, respectively) predicted in [3]. The drift is set as 0.07 so that the simulated average growth rate trajectories align with the predicted demand growth. The volatility is set as 0.05. This value is such that simulated growth rate trajectories are sufficiently dispersed around their averages so that they represent a wide range of possible future scenarios.

In comparison, the traditional stochastic model assumes that demand growth is subject to the normal distribution with a constant variance. This model's PDFs with the same parameters are presented in Fig. 6. As seen, the average value of demand growth increases at a fixed rate, while the variance remains constant. Since the model ignores the increasing variance of demand growth as time elapses, it implicitly assumes that the accuracy of load forecast remains the same over the time horizon. This assumption would incredibly lead to incorrect impacts of demand uncertainty on the network reinforcement deferral or advancement. Since the focus of this paper is to provide investment cost-reflective signals under long-term demand uncertainty, the proposed stochastic model can better capture its stochasticity.

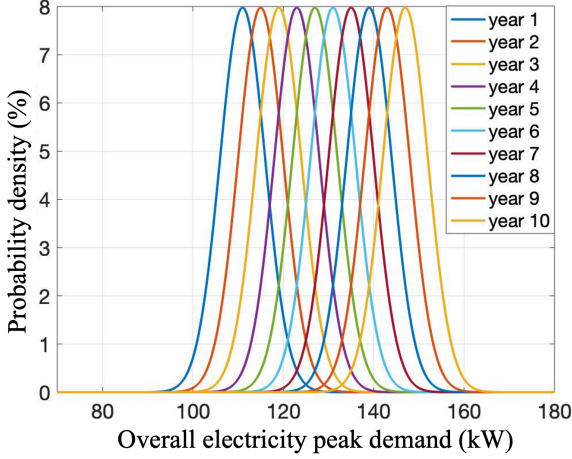


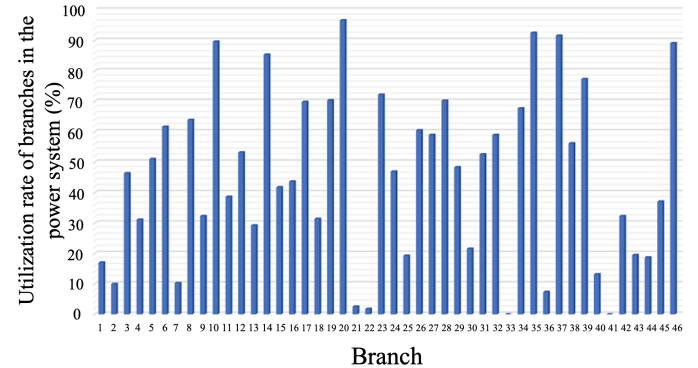
Fig. 6. Probability density distribution of overall electricity peak demand under the normal distribution with constant variance in 10 years. $\mu = 0.07$. $\sigma = 0.05$. $x_0 = 0.2$. The original peak demand in year 0 is 100 kW.

A. Base case

The utilization levels of branches in the power system and pipelines in the gas system in year 0 are shown in Fig. 7. With multi-energy demand varying, the distributions of energy flow inevitably change and thus, the utilization levels of networks change accordingly. The reinforcement is triggered when the utilization level of a network component reaches 100%. The network charges aim to incentivize the efficient utilization of the whole system.

As shown in Fig. 7, branch 20 has the highest utilization rate with 96% in the power system, while branches 33 and 41 have the lowest rate below 1%. In the natural gas system, Pipeline 8 is the most utilized component in the natural gas system. Therefore, if the energy withdrawal of a node has greater

sensitivity to the highly utilized branches or pipelines, its network charges are also high, and vice versa. Because when the utilization is high, the reinforcement becomes imminent and thus leads to a high charge. In comparison, the energy injection that can reduce the loading levels of highly utilized branches contributes to larger negative charges.



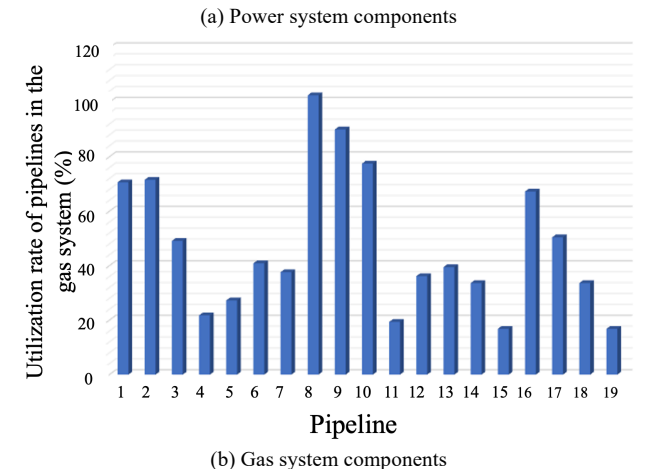


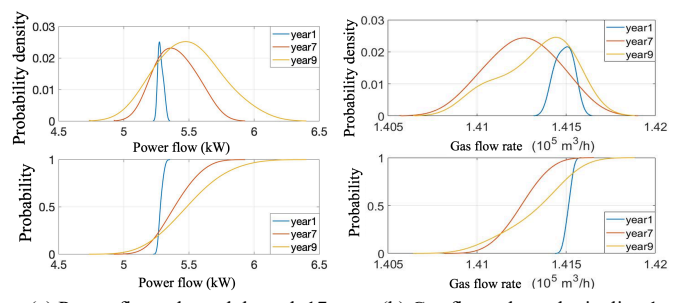
Fig. 7. Original utilization rates of network components in the power system and the gas system in year 0.

The simulation results of the POEF model are probabilistic energy flows through each network component. Fig. 8 is taken as an example to depict the PDF and CDF of power flows through branch 17 and gas flows through pipeline 1 in the 1st, 7th, and 9th years. It can be seen from Fig. 8 (a) that the probability of the power flow falling within 5.25 kW to 5.4 kW in the first year is 100%. Therefore, there are small uncertainties of power flows in the first year. By contrast, in the 7th year, the probable range of energy flows falls within 4.9 kW to 6kW, with a larger variance. In the 9th year, the probable power flow of branch 17 reaches 6.5 kW, with a minimum possible value of 4.75 kW. The figure demonstrates that both the uncertainty and the highest probable power flow of branch 17 rise with time.

Fig. 8 (b) shows the probabilistic gas flow rates through pipeline 1. Similarly, it can be seen from the figure that in the first year, the gas flow rates are between $1.413 \times 10^5 m^3/h$ and $1.417 \times 10^5 m^3/h$, while the variance increases to $1.408 - 1.417 \times 10^5 m^3/h$ in year 7. In the ninth year, the probabilistic gas flow rate falls within 1.406 - 1.418 × $10^5 m^3/h$. Because the long-term uncertainty of energy load growth increases over time, the variance of the probabilistic gas flow function also increases.

Fig. 9 shows the expected loading levels at risk, i.e., TVaRs

of all branches from the first year to the 9th year. It can be found in the figure that the uncertainty of demand growth has a very small impact on the utilization of branches 7, 21, 22, 33, 36, 41, and 46. By contrast, branches 10, 14, 19, 23, 26, 28, 35 have a significant variation in the expected loading levels over time. Therefore, the nodal energy demand which imposes more loads on these branches may be charged more because they can advance the future investment of highly utilized components, vice versa.



(a) Power flows through branch 17 (b) Gas flows through pipeline 1 Fig. 8. PDF and CDF of energy flows through example branches and pipelines.

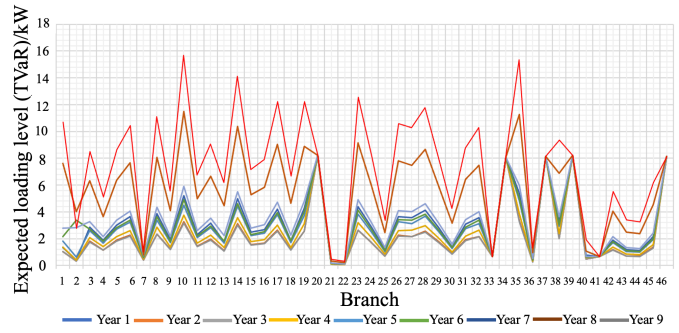


Fig. 9 Expected loading levels for all branches in the power system.

Fig. 10 illustrates the expected gas flow rates for all pipelines in the gas system from the first year to the 9th year. Compared to other pipelines, L5 and L6 have higher risks of overloading, which are much more sensitive to stochastic demand growth over time. Based on TVaRs, the expected loading level, reinforcement horizons and the discounted future investment costs can be calculated. In the base case, the future costs in the power system and gas system due to stochastic energy demand growth are £6.8669m and £0.982m, respectively.

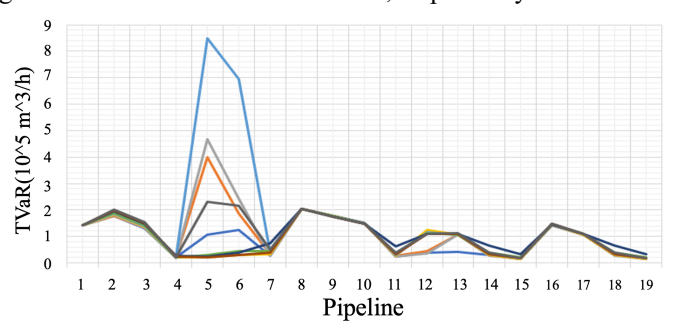


Fig. 10 Expected gas flow rates for all pipelines in the gas system.

Incremental case

The incremental cases demonstrate the impact of nodal energy demand withdrawal or injection on the probabilistic energy flows and the future investment costs, which are used to calculate the annualized network charges. Because Fig. 8.

shows the energy flows of branch L17 and pipeline L1 in the base case as an example, this part selects the same components but in different incremental cases (i.e., incremental energy demand withdrawal on different nodes).

Fig. 11. shows the updated PDF and CDF of power flows through branch 17 with incremental demand (1kW) growth on bus 9 and bus 29 of the power system. The diagrams indicate that the nodal demand increase of bus 24 lifts the maximum power flows of branch 17 from 5.4 kW to 6.3 kW in the first year, from 5.9 kW to 6.3 kW in the 7th year and from 6.45 kW to 6.8 kW in the 9th year. By contrast, the increment of bus 29 has a marginal effect on the loading level of branch 17. Therefore, the nodal energy demand growth of bus 9 can significantly advance the reinforcement of branch L17, leading to a high network charge for the component L17.

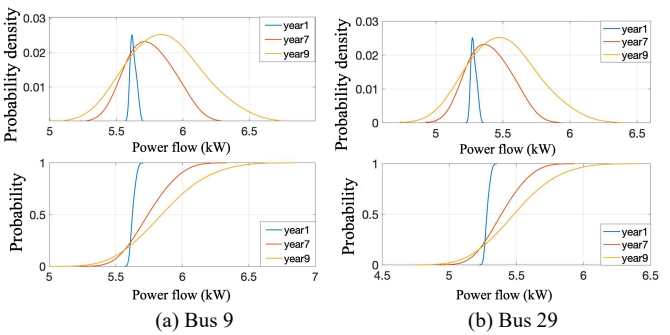


Fig. 11 PDFs and CDFs of power flows through branch 17 with incremental demand at bus 9 and bus 29.

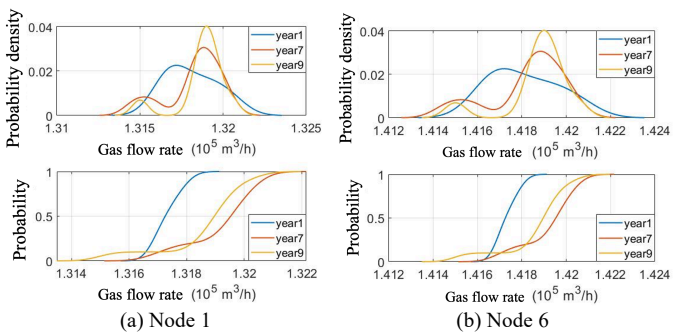
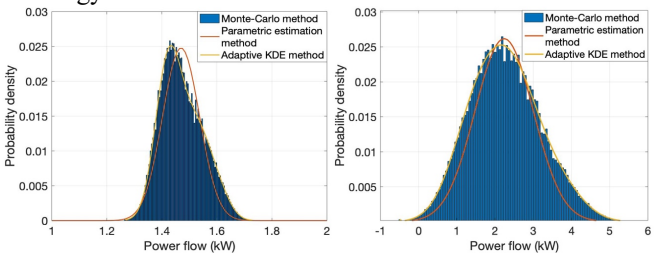


Fig. 12 PDF and CDF of gas flow rates through pipeline 1 with incremental demand at node 1 and node 6.

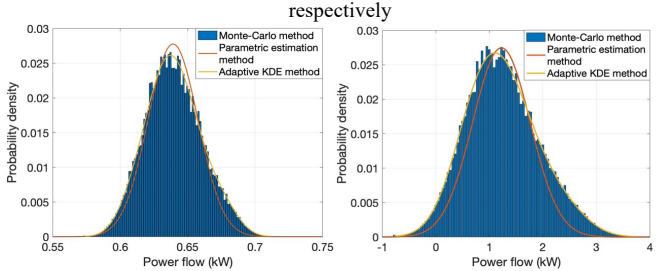
Fig. 12 depicts the effects of incremental gas injection of node 1 and incremental gas demand of node 6 in the gas system on the flow rates of pipeline L1. It can be found that the nodal gas injection of node 1 (i.e., gas well 1) leads to the fall in gas flow rate of pipeline L1 with around $1 \times 10^4 m^3/h$, while the nodal gas withdrawal of node 6 (i.e., the gas generator G4) leads to the rise of around $500m^3/h$. Therefore, the incremental gas injection of node 1 and withdrawal of node 6 will cause negative and positive network charges, respectively, in terms of the reinforcement cost for pipeline L1. In other words, the pricing methodology can reflect the utilization of the system infrastructures in serving incremental energy injection or withdrawal, which are drivers of the investment of MES.

To illustrate the effectiveness of the proposed POEF model, the PDFs of example branches and pipelines are simulated using the Monte-Carlo method, the parametric method and the proposed adaptive KDE method, as shown in Fig.13. It can be seen that the PDFs generated from the proposed method can

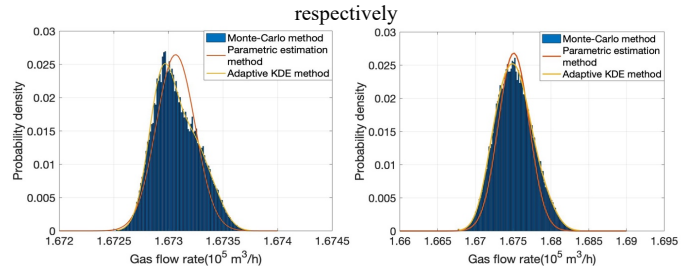
highly align with the simulated probability density distributions under Monte-Carlo simulation, particularly in the tail part. If the probabilistic energy flows are close to a normal distribution, the parametric method also shows an acceptable fitting effect. However, it has a non-ignorable deviation in the tail part, especially when the probability density does not conform to the normal distribution. The results demonstrate the effectiveness of the proposed adaptative KDE-based model in fitting the PDF of energy flows.



(a) The PDFs of power flows through branch 1 in the 1st and 10th year,



(b) The PDFs of power flows through branch 2 in the 1st and 10th year,



(c) The PDFs of gas flow rates through pipeline 1 in the 1st and 10th year, respectively

Fig. 13. PDFs of power flows and gas flow rates under the Monte-Carlo simulation, the parametric method, and the proposed adaptative KDE method.

C. Pricing Results

Table IV shows the breakdown of incremental reinforcement costs with and without nodal energy withdrawal increments and their annual network charges. The incremental cost of network components represents the difference of present values in the expected reinforcement due to nodal demand injection. Specifically, nodal demand injection will change the system's optimal energy flows under contingency. Nevertheless, the impact varies from branch to branch and from pipeline to pipeline. Positive incremental costs of a component c mean that the contingent energy flow of c increases and thus the reinforcement horizon is advanced due to nodal demand injection. Therefore, this nodal demand injection leads to a growth of the present value in the reinforcement cost, i.e., positive incremental costs. Accordingly, positive and negative incremental costs represent investment time advancement and deferral, respectively.

As shown in Table IV, the incremental demand injection at

bus 13 changes energy flow distribution.s It defers the reinforcement of branch L1 and contributes to the decline of the present value in its investment costs by $-2.2875 \times 10^3 \text{E}/MW/yr$. It also results in increasing utilization levels of other network components (e.g., L3, L5, L31) as shown in the table. In the base case, the expected present value in future investment costs is $6.8669 \times 10^4 \text{E}/MW/yr$ in the power system and 98.2 E/MW/yr in the gas system. With incremental electricity demand at bus 13, the present value in future costs grows to $1.0157 \times 10^5 \text{E}/MW/yr$ and $3.11 \times 10^3 \text{E}/MW/yr$, respectively. Therefore, the annual network charge is $32.898 \times 10^3 \text{E}/MW/yr$ and to $2.128 \times 10^3 \text{E}/MW/yr$ in the two systems, which is $3.2898 \times 10^4 \text{E}/MW/yr$ in total.

TABLE IV
BREAKDOWN OF REINFORCEMENT COSTS AND NODAL ANNUAL NETWORK

		CHARGES			
Bus /Node	Branch/ Pipeline	Incremental cost of components (10 ³ £)	Total base cost (10 ³ £)	Total increm ental cost (10 ³ £)	Annual charge (10³£)
	L1 L3,L5,L31 L16 L4,L9,L11,L13, L15,L24,L28,L	-2.2875 0.5419 0.6998	68.669	101.57 0	
Bus13	29,L30,L42,L45 P2,P3,P4, P5,P6,P7, P11,P12,P13,P1 4,P15,P18,P19	0.1637	0.982	3.110	35.026
Bus29	L2 L3 L12 L31	1.6386 0.1687 -0.1928 0.5419	68.669	70.825	4.120
P P	P11,P12,P13,P1 4,P15,P18,P19	0.1637	0.982	2.947	
D 20	L2 L3 L5 L12	0.3491 -2.4454	68.669	68.368	1.60
Bus 30	L31 P3,P4,P5,P6,P7, P11,P12,P13,P1	0.3491	0.982	2.947	1.663
	L5 L2	-0.7391 0.8980	68.669	68.828	
Node N3	P1, P9, P10, P16, P17 P2, P5, P6 P3, P7, P12, P13, P14, P18	-0.7391 1.3401 0.8980	0.982	6.695	6.443
	L33	1.7517	68.669	70.421	
Node	P2	0.0925			
Bus13	7.876	8.837			
	P1,P3,P9,P10,P 11,P12,P13,P16	0.89797	0.982	8.7738	7.7916
NI8	P2	0.09246			
	P5, P6	-0.1913			

The annual network charge of bus 29 is $4.120 \times 10^3 E/MW/yr$. The demand connected at gas node N6 only decreases the utilization levels of pipelines P5 and P6. Thus, it delays the

reinforcement time of P5 and P6 and advances that of other pipelines and branches. The charge of bus 13 is higher than charges of buses 29, 30, and node N6 because bus 13 uses the network more extensively, i.e., it is served by more highly utilized branches and pipelines.

D. Performance Comparison

To demonstrate the benefit of the proposed method, the same case study is performed using the deterministic LRIC method and the traditional method that does not consider the utilization level of the MES network. Table V compares the pricing results with the three methods. The traditional uniform pricing method assumes the existing MES network is fully utilized, i.e., incremental demands at any nodes will contribute to the reinforcement of all network components by the same value. Thus, all nodes are charged at the same amount, i.e., $1.1086 \times 10^4 \text{E}/MW/yr$.

 $\label{thm:comparison} TABLE~V$ Result Comparison with the Proposed Method, Deterministic LRIC

AND TRADITIONAL METHOD				
Bus/Node	Proposed	Deterministic	Traditional	
	method	LRIC method	method	
	$(10^{3} £)$	$(10^{3}£)$	$(10^{3} £)$	
Bus 1	3.773	11.986		
Bus 9	1.965	11.883		
Bus 13	35.026	13.628		
Bus 19	0.683	10.834		
Bus 29	4.120	12.168	11.086	
Bus 30	1.663	11.210		
Node N1	8.553	11.660		
Node N6	8.645	11.912		
Node N19	9.543	12.074		

Although the deterministic LRIC (D-LRIC) method considers the utilized capacity of MES, it assumes that all nodes share the same fixed load growth rates (i.e., 20%), which ignores the long-term uncertainty. In terms of the mentioned nodes and buses in Table V, the charge at bus 33 is the highest with $1.3628 \times 10^4 \text{E}/MW/yr$, while bus 19 has the lowest charge with 1.0834×10^4 £/MW/yr. The buses with the highest and lowest charges from the proposed method are the same with D-LRIC, i.e., bus 13 and bus 19, with 3.5026 × $10^4 E/MW/yr$ and 683 E/MW/yr, respectively. That is because the network is more extensively utilized in serving demands at bus 13. For instance, branches L19, L20, L22, L21, L28 may be needed by generating unit G3 to support incremental demands at bus 13. Especially, as shown in Fig. 7, the existing utilization rate of L20 is the highest with more than 95%. The branches L19 and L28 are also highly utilized with around 70%. By contrast, Bus 19 is served through L33, the utilization rate of which is the lowest, i.e., less than 5%. Thus, the charge for bus 19 is much lower than the others.

The charges calculated from D-LRIC are generally higher than those from the proposed method with less variation among different nodes. It is because D-LRIC presumes a high fixed load growth rate. In reality, however, the load growth rate may be lower or higher than the predefined value. Under long-term uncertainty, the ability to defer reinforcement is more valuable than that under deterministic scenarios [40]. Because the defer option can provide planning flexibility in response to various future conditions [41]. Since bus 13 advances the reinforcement

of L19, L20 and L28 significantly, it kills the option to wait for new information and productively invest in the future. The opportunity cost is ignored in D-LRIC. Therefore, the charge of bus 13 from the proposed method is higher than that from D-LRIC. The charge of bus 19 from the proposed method is lower than that from D-LRIC because demand increments at bus 19 can improve the system's planning flexibility.

E. Pricing sensitivity to load uncertainty

This section investigates the effects of load uncertainty variance (i.e., σ in Fig. 5.) on network pricing results. Fig. 14. shows the pricing results of four nodes with different nodal peak demand variances. It can be observed that the variances of load peak growth increase from 20% to 220%, and the annual charges of Bus 30, Bus 9, Bus 29 and Node N1 grow by around $8 \times 10^4 \text{£}, 3.5 \times 10^4 \text{£}, 2 \times 10^4 \text{£}, \text{ and } 2 \times 10^3 \text{£}, \text{ respectively.}$ The results indicate that with the variance growing, the risks for more investment measures also increase, leading to higher charges for all buses and nodes. Nevertheless, the pricing sensitivity of these components to the variance is different. It can be seen that among the four nodes, Bus 30 is the least sensitive, while Node N1 has the biggest change during the range under study. It is mainly because the incremental demand at Bus 30 contributes a small proportion to the network reinforcement through energy flow growth, while Node N1 contributes a large proportion. In other words, Node N1 utilizes the network most extensively, which leads to a large annual charge at the base variance rate. Therefore, with the variance of load growth, nodal demand increments at Node N1 have a larger impact on the future network reinforcement. The results demonstrate that the investment risks due to load growth uncertainty are shared between all network users. The charges reflect the degree to which the network can serve more demand growth under long-term uncertainty.

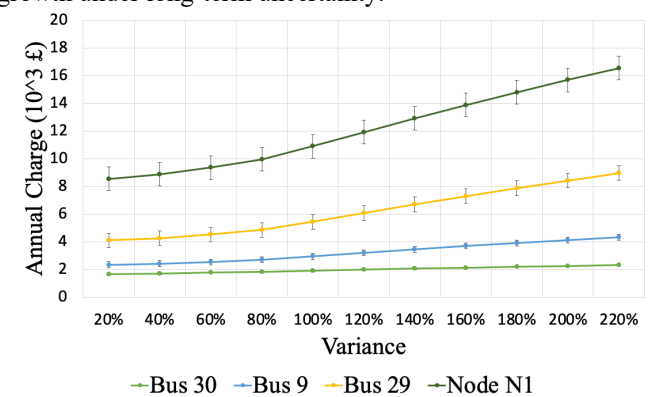


Fig. 14. Incremental charge under different load growth variances

VI. DISCUSSION

In the UK [42] [43], The price control scheme sets expense (i.e., investment) and revenue (i.e., recovery from consumers) allowances for energy network companies. Timely investment and cost recovery methods are needed to ensure the ongoing reliability and resilience of the gas and electricity transmission networks. This paper proposes a long-term network pricing method for MES, which for the first time considers long-term uncertainty of multi-energy demand in pricing signals. Key

findings and achievements can be concluded from simulation results, as shown below:

- 1) The GBM-based model can better capture the stochasticity of uncertain multi-energy demands by considering the varying variance of demand growth rates. The average growth rate trajectory of simulation results aligns with the predicted demand growth scenarios by National Grid. The simulated growth rate trajectories are also sufficiently dispersed around their averages to incorporate a wide range of possible future scenarios. The proposed model enables system operators to analyse the long-term uncertainty on multi-energy system planning and investment.
- 2) The proposed adaptive KDE method shows a good fitting effect for energy flows with long-tailed and non-normal distribution. Results show that the obtained PDFs highly align with those from MSC. Compared with the parametric estimation method, it has a much lower deviation for nonnormal and long-tailed distributions. The model provides a beneficial tool to analyse probabilistic energy flows in a complex system with good accuracy.
- 3) The proposed LRIC-based pricing method can reasonably reflect the effect of nodal incremental loads on the predicted investment horizon of branches and pipelines. The final locational charges indicate how network users utilize the energy network. They reflect where the network can serve more demand without requiring investment. Compared with the traditional uniform pricing method and the deterministic LRIC method, the proposed approach can represent the effect of load growth uncertainty on network development. Results indicate that long-term uncertainty has a negative impact on network utilization and thus leads to higher network charges. The final charges enable system operators to share the investment risks caused by long-term uncertainty with MES customers.

The obtained price signals can achieve the tradeoff of multiple criteria of pricing methods, i.e., cost-reflectivity, predictability and forward-looking signals. Nevertheless, it can be further improved to facilitate a more efficient and fair allocation of network investment costs, allowing for the paradigm shift and increasing uncertain technologies. The future research directions include: i) Carbon signals should be incorporated in the pricing method to incentivize the integration of low-carbon technologies. ii) Flexible demand (e.g., battery storage systems and electric vehicles) should be further investigated in network pricing to ensure that their flexibility values are fairly evaluated and awarded. iii) The proposed pricing model can be extended to generation by modelling the uncertain development of generation capacity and energy mix.

VII. CONCLUSION

This paper proposes an LRIC-based network pricing methodology to guide the development of future demand under the long-term uncertainty of load growth. Case studies indicate that the proposed method has better performance under uncertain circumstances, compared with the traditional method and D-LRIC. The proposed method can not only use nodal charges to reflect the utilized capacity of MES but also provide a forward-looking price signal that reflects the expected

investment costs on MES to supply uncertain multi-energy demand. Moreover, it investigates how different nodal increments of energy injection and withdrawal influence the planning flexibility under long-term uncertainty. Through price signals, the proposed pricing method enables better utilization of the MES network by encouraging efficient siting and sizing of future multi-energy demand and generation.

The proposed method provides an analytical tool to network operators to collect revenues and recover costs. It also enables them to guide better sitting and sizing of demand to minimize investment costs and hedge risks from load growth uncertainty. In this way, the new pricing approach can help achieve more efficient MES planning and cost-effective utilization under long-term uncertainty, thus reducing low-carbon transition costs.

REFERENCES

- [1] N. Good and P. Mancarella, "Flexibility in Multi-Energy Communities With Electrical and Thermal Storage: A Stochastic, Robust Approach for Multi-Service Demand Response," *IEEE Transactions on Smart Grid*, vol. 10, no. 1, pp. 503-513, 2019, doi: 10.1109/TSG.2017.2745559.
- [2] Z. Zhang, R. Li, and F. Li, "A Novel Peer-to-Peer Local Electricity Market for Joint Trading of Energy and Uncertainty," *IEEE Transactions on Smart Grid*, vol. 11, no. 2, pp. 1205-1215, 2020, doi: 10.1109/TSG.2019.2933574.
- [3] "National Grid's Annual Future Energy Scenarios Report," in "System View," National Grid ESO, July,2020 2020.
- [4] W.-W. Kim, J.-K. Park, Y.-T. Yoon, and M.-K. Kim, "Transmission Expansion Planning under Uncertainty for Investment Options with Various Lead-Times," *Energies*, vol. 11, p. 2429, 09/13 2018, doi: 10.3390/en11092429.
- [5] A. Hassan, S. Acharya, M. Chertkov, D. Deka, and Y. Dvorkin, "A Hierarchical Approach to Multienergy Demand Response: From Electricity to Multienergy Applications," *Proceedings of the IEEE*, vol. 108, no. 9, pp. 1457-1474, 2020, doi: 10.1109/JPROC.2020.2983388.
- [6] H. R. Massrur, T. Niknam, and M. Fotuhi-Firuzabad, "Investigation of Carrier Demand Response Uncertainty on Energy Flow of Renewable-Based Integrated Electricity-Gas-Heat Systems," *IEEE Transactions on Industrial Informatics*, vol. 14, no. 11, pp. 5133-5142, 2018, doi: 10.1109/TII.2018.2798820.
- [7] Z. Li, Y. Xu, X. Feng, and Q. Wu, "Optimal Stochastic Deployment of Heterogeneous Energy Storage in a Residential Multienergy Microgrid With Demand-Side Management," *IEEE Transactions on Industrial Informatics*, vol. 17, no. 2, pp. 991-1004, 2021, doi: 10.1109/TII.2020.2971227.
- [8] Z. Li et al., "Probability-Interval-Based Optimal Planning of Integrated Energy System With Uncertain Wind Power," IEEE Transactions on Industry Applications, vol. 56, no. 1, pp. 4-13, 2020, doi: 10.1109/TIA.2019.2942260.
- [9] T. Ding, Y. Hu, and Z. Bie, "Multi-Stage Stochastic Programming With Nonanticipativity Constraints for Expansion of Combined Power and Natural Gas Systems," *IEEE Transactions on Power Systems*, vol. 33, no. 1, pp. 317-328, 2018, doi: 10.1109/TPWRS.2017.2701881.
- [10] E. A. M. Ceseña, T. Capuder, and P. Mancarella, "Flexible Distributed Multienergy Generation System Expansion Planning Under Uncertainty," *IEEE Transactions on Smart Grid*, vol. 7, no. 1, pp. 348-357, 2016, doi: 10.1109/TSG.2015.2411392.
- [11] Y. Chen, W. Wei, F. Liu, E. E. Sauma, and S. Mei, "Energy Trading and Market Equilibrium in Integrated Heat-Power Distribution Systems," *IEEE Transactions on Smart Grid,* vol. 10, no. 4, pp. 4080-4094, 2019, doi: 10.1109/TSG.2018.2849227.
- [12] R. Chen, J. Wang, and H. Sun, "Clearing and Pricing for Coordinated Gas and Electricity Day-Ahead Markets Considering Wind Power Uncertainty," *IEEE Transactions on Power Systems*, vol. 33, no. 3, pp. 2496-2508, 2018, doi: 10.1109/TPWRS.2017.2756984.

[13] S. Chen, G. Sun, Z. Wei, and D. Wang, "Dynamic pricing in electricity and natural gas distribution networks: An EPEC model," *Energy*, vol. 207, p. 118138, 2020/09/15/ 2020, doi: https://doi.org/10.1016/j.energy.2020.118138.

- [14] "Statement of LDZ Transportation Charges," in "Transportation Charges," Wales & West Utilities, 1, April 2021, vol. 3.0.
- [15] L. Cauret, R. Belhomme, P. Raux-Defossez, S. Nösperger, J. Steinbeisser, and J. P. Carpe, "Flexibility provision through enhanced synergies between electricity, gas and heat systems: a comparative analysis of market and regulatory frameworks in seven case study countries," *IET Energy Systems Integration*, vol. 2, no. 2, pp. 133-143, 2020, doi: 10.1049/iet-esi.2019.0062.
- [16] X. Yan, C. Gu, F. Li, and Y. Xiang, "Network pricing for customer-operated energy storage in distribution networks," *Applied Energy*, vol. 212, pp. 283-292, 2018/02/15/ 2018, doi: https://doi.org/10.1016/j.apenergy.2017.12.060.
- [17] P. Cassels, "DNO DUOS Price Setting for the start of RIIOED2," Energy Networks Association, London, 5, May 2021.
- [18] F. Li and D. L. Tolley, "Long-run incremental cost pricing based on unused capacity," *IEEE Transactions on Power Systems*, vol. 22, no. 4, pp. 1683-1689, 2007.
- [19] C. Gu, W. Yang, Y. Song, and F. Li, "Distribution Network Pricing for Uncertain Load Growth Using Fuzzy Set Theory," *IEEE Transactions on Smart Grid*, vol. 7, no. 4, pp. 1932-1940, 2016, doi: 10.1109/TSG.2016.2518175.
- [20] X. Yang, C. Gu, X. Yan, and F. Li, "Reliability-based Probabilistic Network Pricing with Demand Uncertainty," *IEEE Transactions on Power Systems*, pp. 1-1, 2020, doi: 10.1109/TPWRS.2020.2976944.
- [21] E. Mahboubi-Moghaddam, M. Nayeripour, J. Aghaei, A. Khodaei, and E. Waffenschmidt, "Interactive Robust Model for Energy Service Providers Integrating Demand Response Programs in Wholesale Markets," *IEEE Transactions on Smart Grid*, vol. 9, no. 4, pp. 2681-2690, 2018, doi: 10.1109/TSG.2016.2615639.
- [22] C. Luo, Y. Huang, and V. Gupta, "Stochastic Dynamic Pricing for EV Charging Stations With Renewable Integration and Energy Storage," *IEEE Transactions on Smart Grid*, vol. 9, no. 2, pp. 1494-1505, 2018, doi: 10.1109/TSG.2017.2696493.
- [23] W. Jia, T. Ding, C. Huang, Z. Wang, Q. Zhou, and M. Shahidehpour, "Convex Optimization of Integrated Power-Gas Energy Flow Model With Applications to Probabilistic Energy Flow," *IEEE Transactions on Power Systems*, vol. 36, no. 2, pp. 1432-1441, 2021, doi: 10.1109/TPWRS.2020.3018869.
- [24] H. Nosratabadi, M. Mohammadi, and A. Kargarian, "Nonparametric Probabilistic Unbalanced Power Flow With Adaptive Kernel Density Estimator," *IEEE Transactions on Smart Grid*, vol. 10, no. 3, pp. 3292-3300, 2019, doi: 10.1109/TSG.2018.2823058.
- [25] M. Fan, V. Vittal, G. T. Heydt, and R. Ayyanar, "Probabilistic Power Flow Studies for Transmission Systems With Photovoltaic Generation Using Cumulants," *IEEE Transactions on Power Systems*, vol. 27, no. 4, pp. 2251-2261, 2012, doi: 10.1109/TPWRS.2012.2190533.
- [26] S. Chen, Z. Wei, G. Sun, K. W. Cheung, and Y. Sun, "Multi-Linear Probabilistic Energy Flow Analysis of Integrated Electrical and Natural-Gas Systems," *IEEE Transactions on Power Systems*, vol. 32, no. 3, pp. 1970-1979, 2017, doi: 10.1109/TPWRS.2016.2597162.
- [27] A. Qahtan, S. Wang, and X. Zhang, "KDE-Track: An Efficient Dynamic Density Estimator for Data Streams," *IEEE Transactions* on Knowledge and Data Engineering, vol. 29, no. 3, pp. 642-655, 2017, doi: 10.1109/TKDE.2016.2626441.
- [28] B. Khorramdel, C. Y. Chung, N. Safari, and G. C. D. Price, "A Fuzzy Adaptive Probabilistic Wind Power Prediction Framework Using Diffusion Kernel Density Estimators," *IEEE Transactions on Power Systems*, vol. 33, no. 6, pp. 7109-7121, 2018, doi: 10.1109/TPWRS.2018.2848207.
- [29] A. Aboubacar and M. E. Machkouri, "Recursive Kernel Density Estimation for Time Series," *IEEE Transactions on Information Theory*, vol. 66, no. 10, pp. 6378-6388, 2020, doi: 10.1109/TIT.2020.3014797.
- [30] S. Moazeni, W. B. Powell, and A. H. Hajimiragha, "Mean-Conditional Value-at-Risk Optimal Energy Storage Operation in the Presence of Transaction Costs," *IEEE Transactions on Power Systems*, vol. 30, no. 3, pp. 1222-1232, 2015, doi: 10.1109/TPWRS.2014.2341642.

[31] S. N. Neftci, "Value at Risk Calculations, Extreme Events, and Tail Estimation," *The Journal of Derivatives*, vol. 7, no. 3, pp. 23-37, 2000, doi: 10.3905/jod.2000.319126.

- [32] T. Morstyn, A. Teytelboym, C. Hepburn, and M. D. McCulloch, "Integrating P2P Energy Trading With Probabilistic Distribution Locational Marginal Pricing," *IEEE Transactions on Smart Grid*, vol. 11, no. 4, pp. 3095-3106, 2020, doi: 10.1109/TSG.2019.2963238.
- [33] C. Zhang, Y. Xu, Z. Y. Dong, and K. P. Wong, "Robust Coordination of Distributed Generation and Price-Based Demand Response in Microgrids," *IEEE Transactions on Smart Grid*, vol. 9, no. 5, pp. 4236-4247, 2018, doi: 10.1109/TSG.2017.2653198.
- [34] Z. Q. Xie, T. Y. Ji, M. S. Li, and Q. H. Wu, "Quasi-Monte Carlo Based Probabilistic Optimal Power Flow Considering the Correlation of Wind Speeds Using Copula Function," *IEEE Transactions on Power Systems*, vol. 33, no. 2, pp. 2239-2247, 2018, doi: 10.1109/TPWRS.2017.2737580.
- [35] E. S. Schwartz and L. Trigeorgis, Real options and investment under uncertainty: classical readings and recent contributions (The MIT Press) (Classical Readings and Recent Contributions). London: MIT Press, 2004.
- [36] "Identifying energy efficiency improvements and saving potential in energy networks," in "Interim Report," Tractebel Engineering, Ecofys, 22, July 2015.
- [37] P. J. Green and A. H. Seheult, "Density Estimation for Statistics and Data Analysis," *Journal of the Royal Statistical Society: Series C (Applied Statistics)*, vol. 37, no. 1, pp. 120-121, 1988, doi: https://doi.org/10.2307/2347507.
- [38] "EHV CHARGING METHODOLOGY (FCP MODEL)," 2020, doi: https://www.dcusa.co.uk/wp-content/uploads/2020/04/SCHEDULE-17-v12.1.pdf.
- [39] T. Jiang, H. Deng, L. Bai, R. Zhang, X. Li, and H. Chen, "Optimal energy flow and nodal energy pricing in carbon emission-embedded integrated energy systems," *CSEE Journal of Power and Energy Systems*, vol. 4, no. 2, pp. 179-187, 2018, doi: 10.17775/CSEEJPES.2018.00030.
- [40] N. Aguiar, V. Gupta, and P. P. Khargonekar, "A Real Options Market-Based Approach to Increase Penetration of Renewables," *IEEE Transactions on Smart Grid*, vol. 11, no. 2, pp. 1691-1701, 2020, doi: 10.1109/TSG.2019.2942258.
- [41] S. Muzzioli and B. D. Baets, "Fuzzy Approaches to Option Price Modeling," *IEEE Transactions on Fuzzy Systems*, vol. 25, no. 2, pp. 392-401, 2017, doi: 10.1109/TFUZZ.2016.2574906.
- [42] J. Veaney, "RIIO-ED2 Methodology Consultation: Overview," Network Price Controls, ofgem, London, 30, July 2020.
- [43] R. Team, "RIIO-2 Draft Determinations Gas Transmission Annex," Network Price Controls, ofgem, London, 9, July 2020.



Shuang Cheng (S'19) received the B.Eng. and MPhil degree in electrical and electronic engineering from North China Electric Power University, Beijing, China in 2017 and 2020, respectively. She received the MSc. degree from the University of Bath, Bath, UK in 2019. She was a visiting scholar in Wroclaw University of Science and Technology. She is currently pursuing the Ph.D. degree with the University of Bath. Her main research interests include energy system planning, power system economics, and market design.



Chenghong Gu (M'14) was born in Anhui province, China. He received the Bachelor's degree from the Shanghai University of Electric Power, Shanghai, China, in 2003, and the Master's degree from the Shanghai Jiao Tong University, Shanghai, China, in 2007, both in electrical engineering. He received the Ph.D. degree from the University of Bath, U.K. He is currently a Lecturer and EPSRC Fellow with the Department of Electronic and Electrical Engineering, University of Bath. His major research interest is in multi-vector energy system, smart grid, and power economics.



Xinhe Yang was born in Fujian, China. He received the B.Eng. degree in electrical and electronic engineering from the University of Bath, Bath, U.K., and the B.Eng. degree in electrical power engineering from North China Electric Power University, Baoding, China, both in 2016. He received the Ph.D. degree in electronic and electrical engineering with the University of Bath in 2022. His main research interests include multicarrier energy systems and smart grids.



Shuangqi Li (Student Member, IEEE) was born in Beijing, China. He received the B.Eng. degree in vehicle engineering from the Beijing Institute of Technology, Beijing, China, in 2018. He is currently working toward the Ph.D. degree in electrical engineering with the Department of Electronic and Electrical Engineering, University of Bath, Bath, U.K. He was a Research Assistant with the National Engineering Laboratory for Electric Vehicles, Beijing Institute of Technology, Beijing, from 2018 to 2019. His major research interests include the big data

analysis, deep-learning algorithm, operation and planning of smart grid systems, and V2G service.



Lurui Fang received the B.Eng. degree in electrical power engineering from the Chongqing University of Science and Technology, Chongqing, China, in 2013, and the M.Sc. degree in electrical power engineering from the University of Southampton, Southampton, U.K., in 2014. He recieved the Ph.D. degree at the University of Bath, Bath, U.K, in 2021. His research focuses on the phase imbalance in low-voltage distribution networks.



economics.

Furong Li (SM'09) received the B.Eng. degree in electrical engineering from Hohai University, Nanjing, China, in 1990, and the Ph.D. degree in electrical engineering from Liverpool John Moores University, Liverpool, U.K., in 1997, with a dissertation on applications of genetic algorithms in optimal operation of electrical power systems. She is currently a Professor and the Director of the Center for Sustainable Power Distribution, University of Bath, Bath, U.K. Her major research interests include the area of power system planning, analysis, and power system